Supplementary Information

Title: Mechanistic Insights into Energy Conservation by Flavin-Based Electron Bifurcation

Authors: Carolyn E. Lubner[1], David P. Jennings[2], David W. Mulder[1], Gerrit J. Schut[3], Oleg A. Zadvornyy[4], John P. Hoben[5], Monika Tokmina-Lukaszewska[4], Luke Berry[4], Diep M. Nguyen[3], Gina L. Lipscomb[3], Brian Bothner[4], Anne K. Jones[2], Anne-Frances Miller[5], Paul W. King[1], Michael W.W. Adams[3], and John W. Peters[4*]

Affiliations:

[1]Biosciences Center, National Renewable Energy Laboratory, Golden, CO 80401.

[2]School of Molecular Sciences, Arizona State University, Tempe, AZ 85287.

[3]Department of Biochemistry and Molecular Biology, University of Georgia, Athens, GA 30606.

[4]Department of Chemistry and Biochemistry, Montana State University, Bozeman, MT 59717.

[5]Department of Chemistry, University of Kentucky, Lexington, KY 40506.

Nature Chemical Biology doi:10.1038/nchembio.2348

Supplementary Results

Supplementary Tables

Table 1.

Data collection and refinement statistics.

	NfnI (Ta peak)	NfnI (Pt peak)	NfnI (Fe peak)	NfnI (as purified)	NfnI NADP(H) bound
Data collection					
Wavelength (Å)	1.25	1.07	1.72	0.88	0.88
Space group	$P3_221$	$P3_221$	$P3_221$	$P3_221$	$P3_221$
Cell dimensions					
a, *b*, *c* (Å)	179.96, 179.96, 80.72	180.11, 180.11, 81.11	180.03, 180.03, 80.80	179.90, 179.90, 80.79	179.70, 179.70, 80.67
α, β, γ (°)	90, 90, 120	90, 90, 120	90, 90, 120	90, 90, 120	90, 90, 120
Resolution (Å)	39-2.11	50-2.04	90-2.7	47.6-1.6	47.5-1.5
R_{merge}	4.4 (8.5)	6.6 (53.2)	13.3 (28.3)	5.8 (48.0)	6.55 (55.7)
$I / \sigma I$	42.9 (15.8)	23.9 (1.3)	26.5 (18.9)	29.5 (4.0)	30.4 (2.7)
Completeness (%)	98.8 (91.8)	96.9 (90.1)	100 (99.8)	100 (99.9)	99.8 (98.4)
Redundancy	3.1 (2.2)	3.3 (2.1)	32.3 (32.1)	8.3 (7.6)	9.1 (5.8)
Refinement					
Resolution (Å)	39-2.11	30.4-2.04	56-2.75	47.59-1.6	47.52-1.5
No. reflections	85978	94828	39360	197382	234804
R_{work} / R_{free}	17.3/19.5	17.9/20.6	14.1/17.6	16.6/17.6	16.1/17.4
No. atoms					
Protein	5851	5851	5851	5851	5851
Ligand/ion	156	156	156	156	229
Water	1030	1030	1030	1032	1046
B-factors					
Protein	26.2	28.5	27.5	19.32	20.48
Ligand/ion	21.5	18.3	22.3	10.9	20.62
Water	37.5	37.1	38.1	36.7	36.43
R.m.s deviations					
Bond lengths (Å)	0.008	0.009	0.008	0.009	0.014
Bond angles (°)	1.1	1.2	1.1	1.3	1.6

*Values in parentheses are for highest-resolution shell.

Table 2.

The k_{cat} for purified *Pf* Nfn compared to published values for Nfn isolated from *Thermotoga maritima* and *Clostridium kluyveri*.

	k_{cat} (s^{-1})			
	Pf NfnI		[2]*Ck* Nfn	[3]*Tm* Nfn
[1]Substrate	Protein film voltammetry (60 °C)	Solution assays (80 °C)	Solution assays (37 °C)	Solution assays (45 °C)
$NADP^+$	108	ND	ND	ND
NAD^+	30	ND	ND	ND
NADPH	16	59	20	ND
NADH	22	10.2	0.8	ND
NADPH + Fd_{ox}	ND	1.3	0.1	0.01
$NADP^+$ + Fd_{red}	ND	11.0	0.3	0.1
$NADP^+$ + NADH + Fd_{red}	11	131	37	6
NADPH + NAD^+ + Fd_{ox}	ND	206	[4]11 or 31	[4]3 or 5

[1]Solution assays of single substrates are dye-linked assays using benzyl viologen. Electron bifurcation experiments require ferredoxin in solution assays, which is omitted in protein film voltammetry experiments, i.e. the electrode serves this function. Buffer pH 7. Values indicate the best measured rate (n = 1). ND = not determined.

[2] Data from [1].

[3] Data from [2].

[4] Determined from absorbance of NADH or Fd, respectively.

Table 3.

Reduction potentials of *Pf* NfnI Flavins.

[1]FAD couple	[2]S-FAD		[3]L-FAD
	DHODB (mV)	***Pf* NfnI (mV)**	***Pf* NfnI (mV)**
$E_{OX/SQ}$	-301	-300.5	-911
$E_{OX/HQ}$	-276.5	-276	-276
$E_{SQ/HQ}$	-252	-251.5	359

[1] OX=oxidized, SQ=semiquinone (general term for the $1e^-$ reduced form of S-FAD or L-FAD), and HQ=hydroquinone (the $2e^-$ reduced form of both S-FAD and L-FAD).

[2] DHODB=dihydroorotate dehydrogenase B. The measured values for the OX/SQ and SQ/HQ reduction potentials of DHODB are shown[3], and the OX/HQ was calculated using $E_{OX/HQ} = ½(E_{OX/ASQ}) + ½(E_{ASQ/HQ})$. DHODB has homology with Nfn-S. The DHODB values were used to derive the corresponding values for *Pf* NfnI S-FAD reduction potentials by the same equation as above, based on the $\Delta E = \pm 24.5$ mV for each $1e^-$ couple of DHODB.

[3] The OX/HQ values for L-FAD and S-FAD are measured for *Pf* NfnI by square wave voltammetry (SWV, Fig. 3C; values are vs. NHE, pH 8). The L-FAD OX/SQ reduction potential is estimated to be -911 mV calculated from fits to $\log k_{ET} = 13 - \beta/2.303 \times (R-3.6) - \gamma \times (\Delta G + \lambda)^2/\lambda = 1 \times 10^{11}\ s^{-1}$ for the measured electron transfer from L-FAD ASQ to the proximal [4Fe-4S] cluster by TAS (Fig. 3D). $\beta = 1.1$, $\gamma = 3.1$, and $\lambda = 0.7$ eV [4]. The Moser-Dutton electron transfer equation is described in [4]; β is a correction factor of the distance parameter that is proportional to the barrier height, γ is the nuclear term parameter, and λ is the reorganization energy parameter. The assumed values for each are based on averages of electron transfer reactions measured for several enzymes as described in [4]. The L-FAD SQ/HQ value is calculated using the equation in footnote 2.

Table 4.

Thermodynamic and kinetic parameters of electron transfer in *Pf* NfnI.

[1]D→A	[2]E_{m8} D (mV)	E_{m8} A (mV)	[3]ΔG (V)	[4]R (Å)	[5]*Nuclear Factor*	[6]*Therm. Factor*	[7]k_{ET} (s^{-1})
Exergonic Pathway							
1. L-FAD_{HQ}→[2Fe-2S]	359	80	0.28	13.1	4.5	4.2	2×10^4
4. [2Fe-2S]→S-FAD_{OX}	80	-300.5	0.38	9.6	2.9	5.2	9×10^4
S1. L-FAD_{ASQ}→[2Fe-2S]	-911	80	-0.99	13.1	4.5	0.4	1×10^8
Endergonic Pathway							
2. L-FAD_{ASQ}→$[4Fe\text{-}4S]_p$	-911	-718	-0.19	5.4	0.9	1.1	1×10^{11}
3. $[4Fe\text{-}4S]_p$→$[4Fe\text{-}4S]_d$	-718	-513	-0.21	9.6	2.9	1.1	1×10^9
S2. L-FAD_{HQ}→$[4Fe\text{-}4S]_p$	359	-718	1.08	5.4	0.9	14.0	1×10^{-2}

[1] D = donor, A = acceptor, p = proximal, d = distal. The schematic (right) shows the sequence of numbering for the electron transfer reactions in the first column. Bifurcating electron transfer reactions are in green (exergonic) and blue (endergonic), and short circuit reactions are in red. S1 is a short circuit that could compete with L-FAD_{ASQ}→$[4Fe\text{-}4S]_p$ ($\sim 10^8$ s^{-1} vs. 10^{11} s^{-1}) and represents two electrons transferred to the exergonic branch. S2 is a short circuit that could compete with the L-FAD_{HQ}→[2Fe-2S] ($\sim 10^{-2}$ s^{-1} vs. $\sim 10^4$ s^{-1}) and represents the first oxidation of fully reduced L-FAD transferred to the endergonic branch.

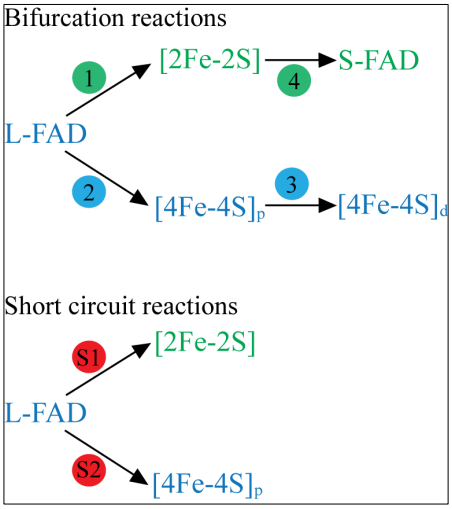

[2] E_{m8} = reduction potential at pH 8. E_{m8} of S-FAD and L-FAD from Table 3; L-FAD_{OX}, $[4Fe\text{-}4S]_p$ and $[4Fe\text{-}4S]_d$ from Fig. 3C; [2Fe-2S] is taken from [5].

[3] $\Delta G = E_{m8}D\ (V) - E_{m8}A\ (V)$.

[4] R is the edge-to-edge distance from the *Pf* NfnI structure. For electron transfer from L-FAD, it is taken as the distance from the O-atom of C2 of L-FAD to the S atom of Cys101 (Nfn-L) of $[4Fe\text{-}4S]_p$, and from C8 atom of L-FAD to the S atom of Cys243 (Nfn-S) of [2Fe-2S].

[5] Nuclear factor = $\beta/(2.303\times(R-3.6))$.

[6] Thermodynamic factor = $\gamma\times[(\Delta G + \lambda)^2/\lambda]$.

[7] $\log k_{ET} = 13 - \beta/2.303\times(R-3.6) - \gamma\times(\Delta G + \lambda)^2/\lambda$; where $\beta = 1.1$, $\gamma = 3.1$, and $\lambda = 0.7$ eV. See Table 3 footnotes for explanation of parameters.

Supplementary Figures

Supplementary Figure 1.

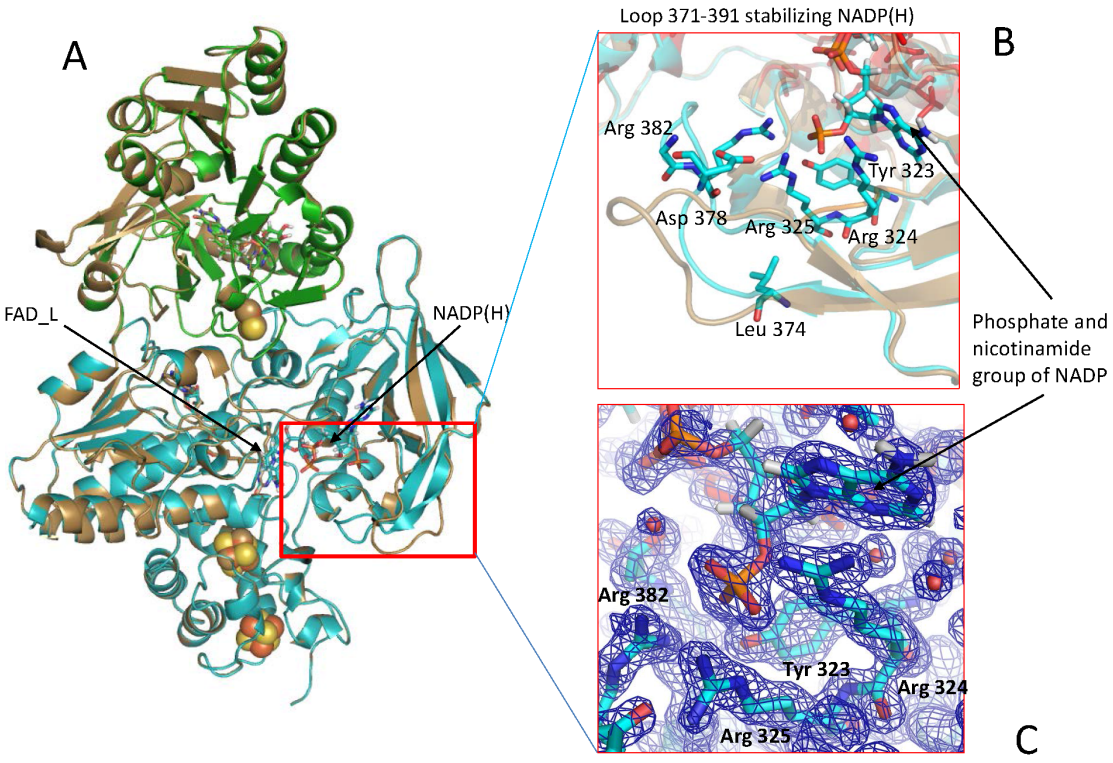

Supplementary Figure 1. Binding of NADP(H) at NfnI-L binding site. (**A**) Cartoon representation of two *Pf* NfnI superposed structures: as-purified (light brown) and NADP(H) bound (Nfn-S in green, and NfnI-L in blue). (**B**) The loop 371-391 of NfnI-L is stabilized by bound NADP(H). The phosphate and adenine groups of the NADP(H) are ligated by the Tyr323, Arg324, Arg325, and Arg382, conserved among the enzymes of the Fnr family. (**C**) Electron density map around residues and bound NADP(H) are shown in blue mesh. The residues involved in the stabilization of the phosphate and nicotinamide group of NADP(H) are shown in sticks. The iron-sulfur clusters are shown in spheres (*yellow,* sulfur; *brown*, iron).

Supplementary Figure 2.

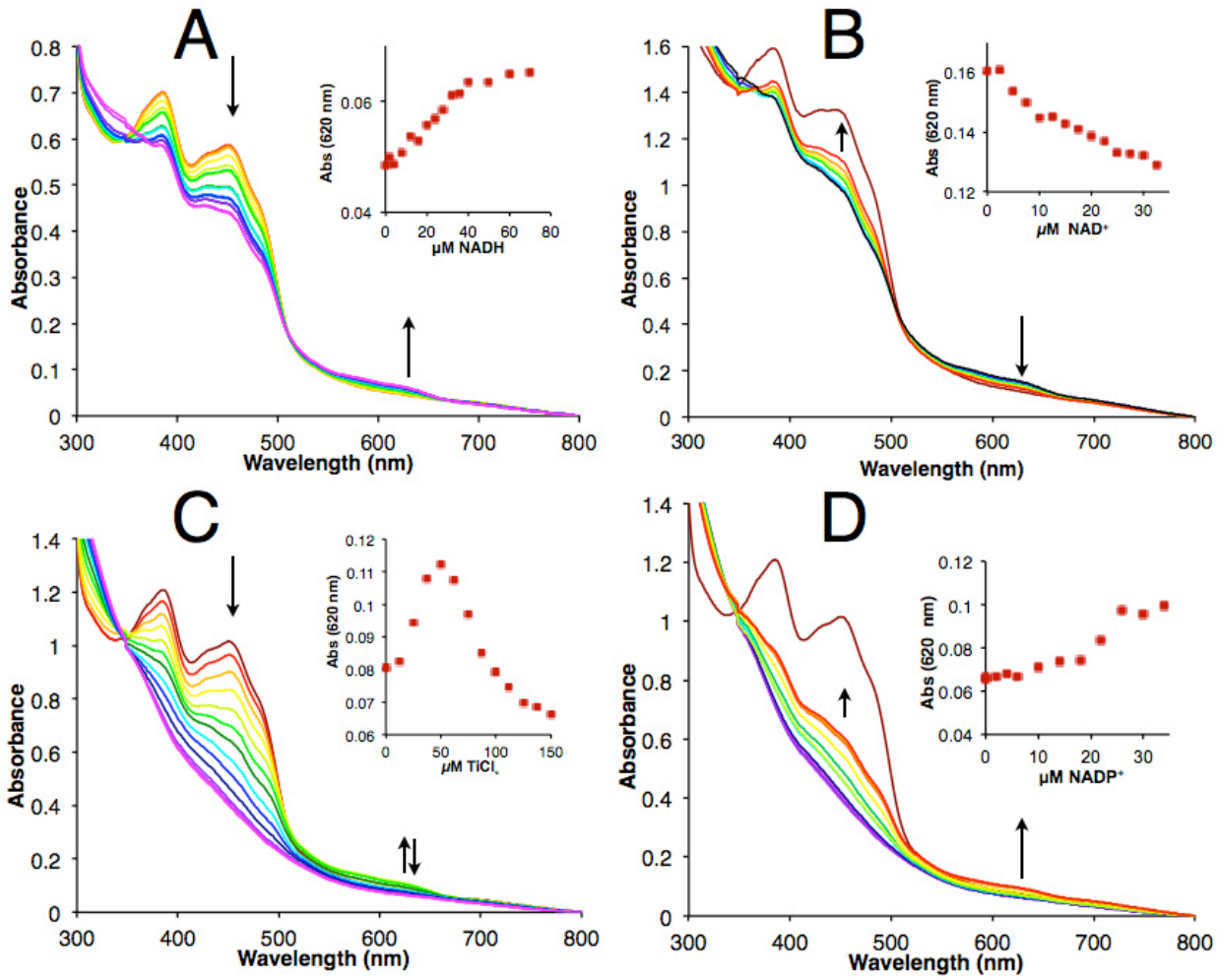

Supplementary Figure 2. Titrations of *Pf* NfnI demonstrating reduction and oxidation of S-FAD. Singly reduced S-FAD NSQ is observed as a broad absorption centered around 620 nm. Arrow shows direction of absorbance change. Insets show changes in NSQ A_{620} as a function of reductant (**A**, **C**) or oxidant (**B**, **D**) concentration. (**A**) A stable NSQ species of S-FAD is formed by reductive titration with increasing amounts of NADH under steady-state conditions; $S\text{-}FAD_{OX}$ + NADH → NAD^+ + $S\text{-}FAD_{NSQ}$ (13 μM *Pf* NfnI, 0 to 70 μM NADH). (**B**) NAD^+ oxidative

titration of *Pf* NfnI reduced with 25 μM NADPH in the presence of stoichiometric amounts of oxidized Fd. S-FAD NSQ is present at the start of the titration (black trace), and decreases as S-FAD becomes oxidized by increasing amounts of NAD^+, according to the bifurcating reaction: $2NADPH + Fd_{OX} + NAD^+ \rightarrow 2NADP^+ + H^+ + Fd_{red} + NADH$ (16.5 μM *Pf* NfnI, 0 to 70 μM NAD^+). (**C**) A stable NSQ species of S-FAD is also formed during reductive titration with the low potential chemical reductant Ti-citrate, however S-FAD NSQ becomes fully reduced to HQ over the course of the titration as seen by the loss of intensity at A_{620}, (16 μM *Pf* NfnI, 0 to 150 μM Ti-citrate). (**D**) $NADP^+$ oxidative titration of *Pf* NfnI that was fully reduced with 150 μM Ti-citrate (sample from **C**). The S-FAD HQ is oxidized to NSQ with electron transfer to $NADP^+$ bound at L-FAD through reverse electron transfer along the exergonic pathway $S\text{-}FAD_{HQ} + NADP^+ \rightarrow NADPH^+ + S\text{-}FAD_{NSQ}$ (16 uM *Pf* NfnI, 0 to 34 μM $NADP^+$).

Supplementary Figure 3.

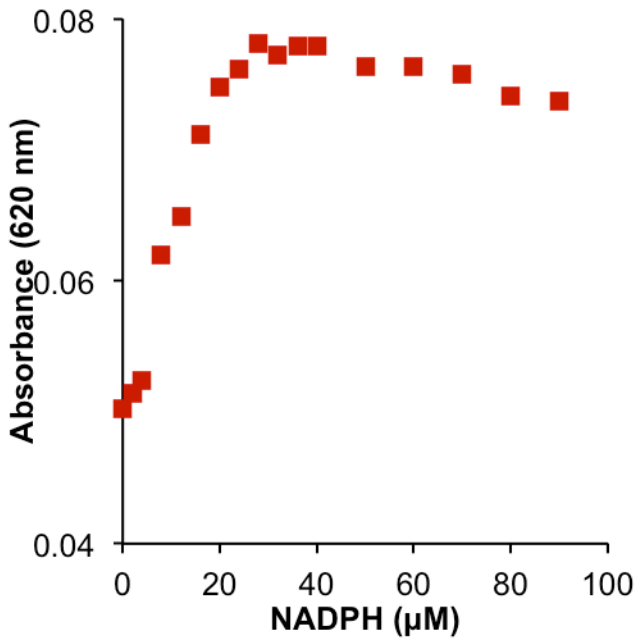

Supplementary Figure 3. A stable NSQ is formed at *Pf*NfnI S-FAD.

An increase in S-FAD NSQ (A_{620} nm) as a function of NADPH concentration is observed during reductive titration of *Pf*NfnI with NADPH under steady-state conditions.

Supplementary Figure 4.

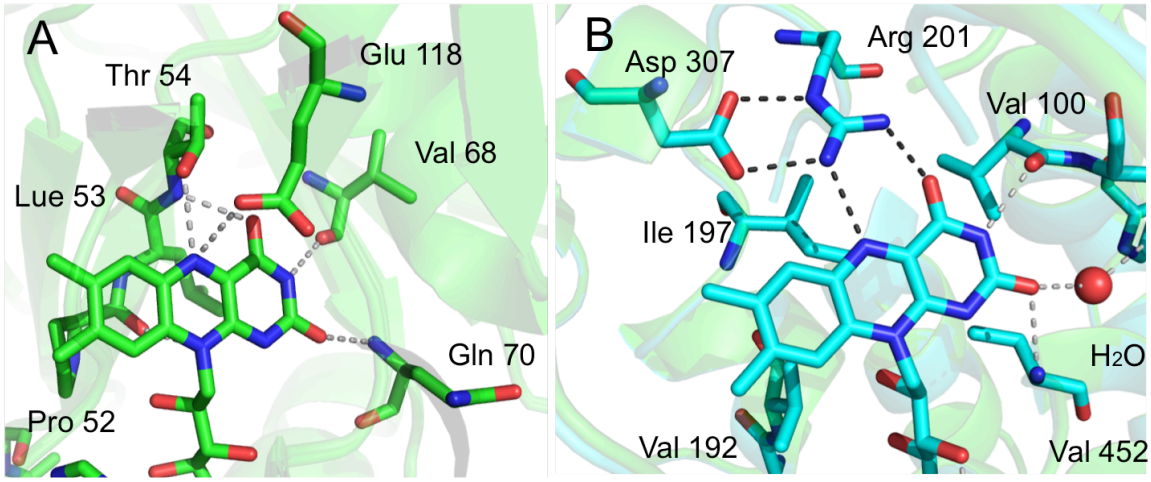

Supplementary Figure 4. Interactions at the isoalloxazine N5 atom of S-FAD and L-FAD. (**A**) The isoalloxazine ring of the S-FAD is flanked from the *si*-face by the side chains of Pro52, Leu53, Val68, and from the *re*-face by Glu118. The N5 and O2 atoms of the isoalloxazine ring are hydrogen bonded to OG and NH atoms of Thr54, and Gln70, respectively. (**B**) The isoalloxazine ring of L-FAD is flanked from the *si*-side face by the side chains of Val100, Val192, Ile197, and from the *re*-face by Val452. The guanidinium NH1 and NH2 groups of Arg201 interact with N5 and O4 of L-FAD, respectively. Asp307 is salt bridged to Arg201. Hydrogen bonds are shown in dashed lines.

Supplementary Figure 5.

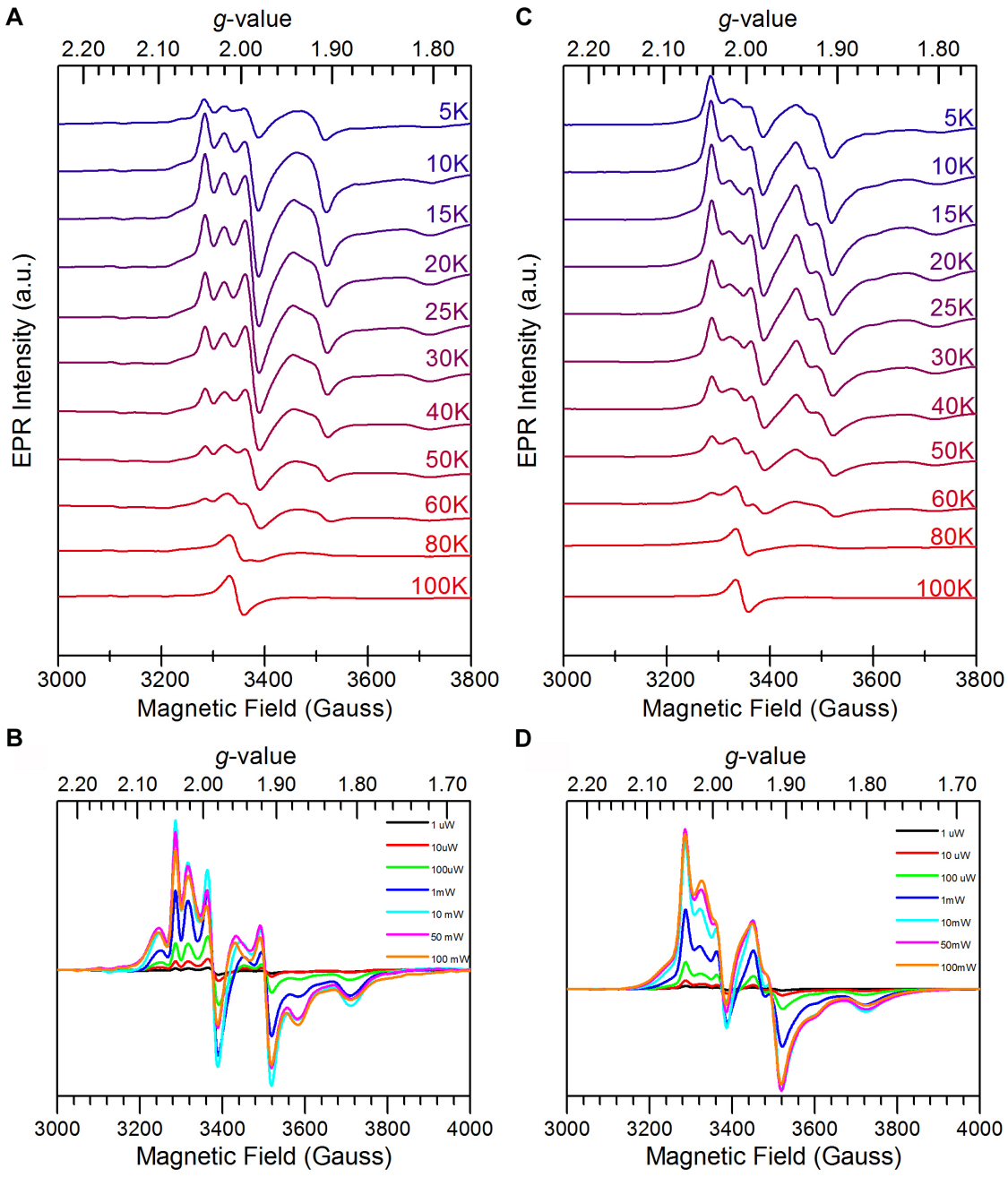

Supplementary Figure 5. Analysis of *Pf* NfnI EPR signals from NADH and NADPH treatments. Temperature series (at 1 mW microwave power) and power dependence (at T = 20

K) of EPR signals from NADH (**A, B**) and NADPH (**C, D**) treatments, respectively. Both treatments demonstrate bifurcation showing similar overlapping rhombic signals that can be assigned to $[2Fe\text{-}2S]^+$ (g = 2.047, 1.915, 1.805) and $[4Fe\text{-}4S]^+$ (g = 2.04, 1.94, 1.90) clusters, as well as a signal that can be assigned to a spin interacting $[2Fe\text{-}2S]^+$ cluster and S-FAD NSQ radical species (g = 2.02, 1.99). In addition, a rhombic signal at g = 2.07, 1.87, 1.80 was identified and can be assigned to the $[4Fe\text{-}4S]^+$ of *Pf* Fd[6], which was present in these samples. The temperature series shows the spin interacting $[2Fe\text{-}2S]^+$ cluster and S-FAD NSQ radical species is most intense between 20 K and 25 K, after which it gradually begins to broaden and resolve to a more uniform isotropic signal centered at g = 2.004 above 80 K. The $[2Fe\text{-}2S]^+$ cluster signal, consistent with previous reports[7], shows similar temperature dependence and is most intense between 20 K and 25 K. At 60 K, the signal is significantly broadened and it is not observed above 80K. The $[4Fe\text{-}4S]^+$ cluster signal is most intense between 15 K and 20 K and detected up to 60 K. While the overall signal intensity is similar between NADH (2.2 spins mol^{-1} at 15 K, 1 mW) and NADPH (2.3 spins mol^{-1} at 15 K, 1 mW), the two treatments show slightly altered distribution of the spin centers. The $[4Fe\text{-}4S]^+$ cluster signal is more intense from the NADPH treatment, while the spin interacting $[2Fe\text{-}2S]^+$ cluster and S-FAD NSQ radical species is more intense from the NADH treatment. These differences are reflected in the power dependence series that show altered power saturation of the overlapping signals.

Supplementary Figure 6.

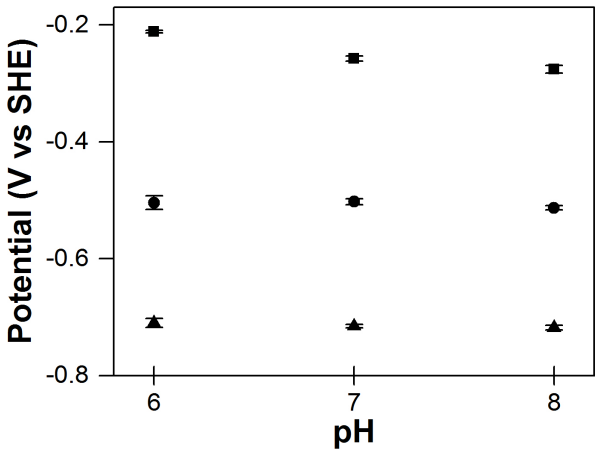

Supplementary Figure 6. pH dependency of *Pf* NfnI flavins.

Dependence of the peaks from square wave voltammetry of immobilized *Pf* NfnI on pH. Squares represent the peak around -200 mV. Circles represent the peak around -500 mV. Triangles represent the peak around -700 mV. Error bars indicate the standard deviation of three repeats.

Supplementary Figure 7.

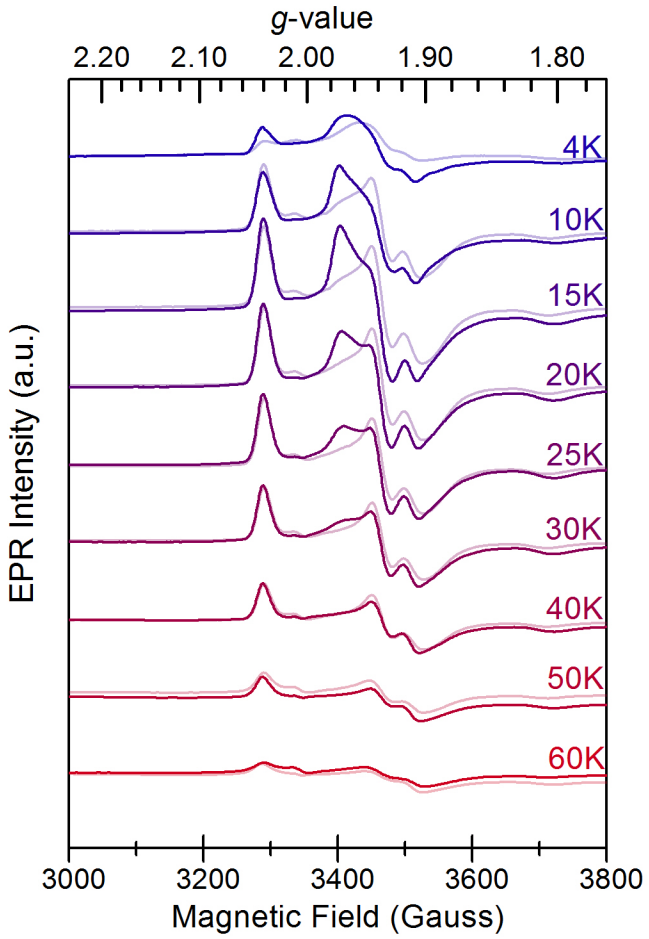

Supplementary Figure 7. Comparison of the temperature series of *Pf* NfnI EPR signals from reduction by sodium dithionite at different potentials. The differential reduction by sodium dithionite allows for deconvolution of two $[4Fe\text{-}4S]^{+}$ cluster signals due to differing midpoint potentials. The spectra show a $[2Fe\text{-}2S]^{+}$ cluster signal (g = 2.047, 1.915, 1.805) along with closely overlapping $[4Fe\text{-}4S]^{+}$ cluster signals (g = 2.04, 1.96, 1.93; g = 2.04, 1.94, 1.90). Reduction by sodium dithionite prepared at -510 mV (darker shades) causes an increase in the overall signal intensity (1.8 spins mol^{-1} at 15 K) compared to reduction by sodium dithionite

prepared at -488 mV (lighter shades, 1.2 spins mol^{-1} at 15 K). The increased intensity can be attributed to $[4Fe\text{-}4S]^{+}$ signal (g = 2.04, 1.96, 1.93) growing in upon reduction. Likewise, this signal appears more intense by reduction with Ti-citrate, which also gives a significant increase in the intensity of the overall signal (6.9 spins mol^{-1}). The increased signal intensity can be partially attributed to Ti-citrate itself, which prevents a detailed analysis for this treatment[8]. The temperature dependence from the sodium dithionite reductions also illustrates the two $[4Fe\text{-}4S]^{+}$ clusters have different relaxation properties. The signal at g = 2.04, 1.96, 1.93 is most intense at 15 K, broadens at 20 K, and is undetectable above 30 K. The other signal at g = 2.04, 1.94, 1.90 is more unusual for $[4Fe\text{-}4S]^{+}$ clusters and can be detected up to 60 K.

Supplementary Figure 8.

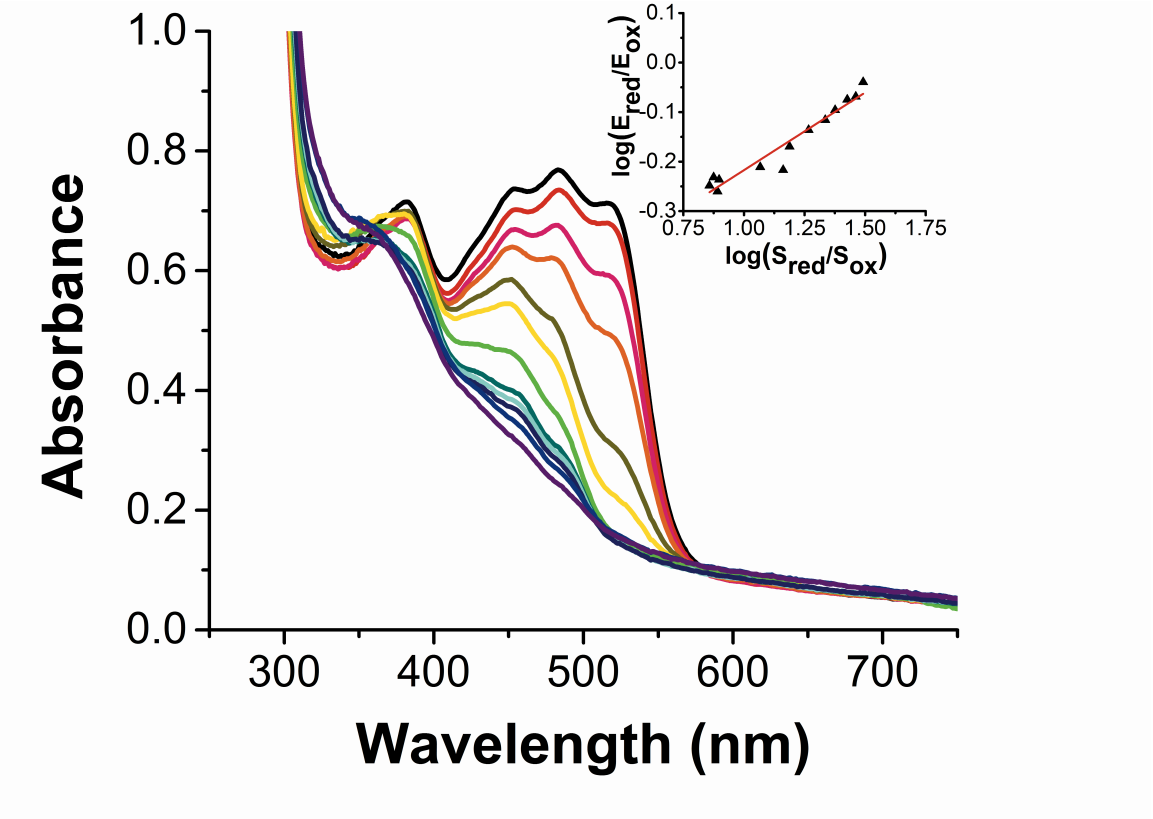

Supplementary Figure 8. Spectroelectrochemical redox titration of *Pf* NfnI. The traces show the anaerobic reduction of *Pf* NfnI (black trace, oxidized; violet trace, reduced). The observation of a single flavin isobestic point near 355 nm indicates direct two-electron reduction to HQ. Based on equilibrium with phenosafranine, the estimated FAD $E_{OX/HQ}$ midpoint potential is -326 vs. NHE (pH 8.0). The inset shows the fit of $\log(E_{red}/E_{ox})$ versus $\log(S_{red}/S_{ox})$ plot for the reduced (red) and oxidized (ox) concentrations of enzyme (E) and standard redox dye (S) for the portion of the reduction where both enzyme and dye undergo similar amounts of reduction (linear fit: adjusted R^2= 0.90).

Supplementary Figure 9.

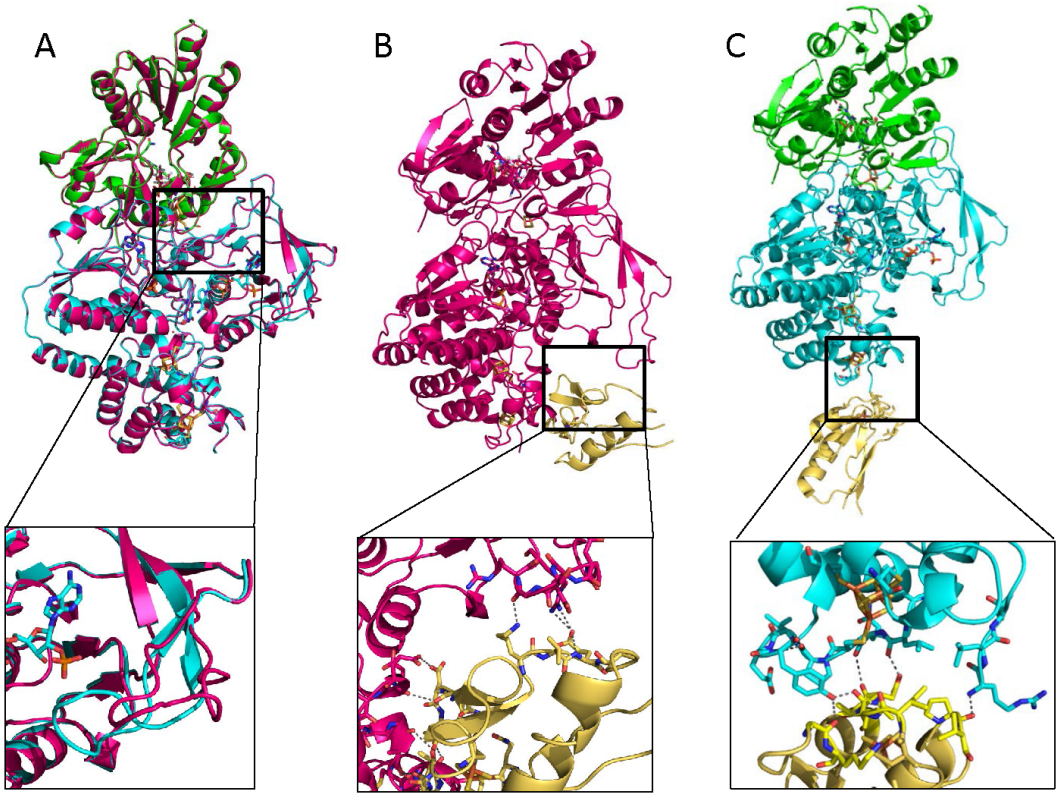

Supplementary Figure 9. Proposed Fd binding site conformational change upon NADP(H) binding at L-FAD. (**A**) Cartoon representation of two *Pf* NfnI superimposed structures: as-purified (magenta) and NADP(H) bound (NfnI-S in green, and NfnI-L in blue). The loop 371-391 of NfnI-L is stabilized by bound NADP(H) in a "closed" conformation, whereas it is in an "open" conformation in the as-purified *Pf* NfnI structure, with B and xyz displacement of 74.5% and 2.1 Å, respectively. (**B**) and (**C**) Computational models (top) of protein-protein docking of *Pf* Fd (PDB code, 1sj1) with as-purified (**B**) or NADP(H) bound (**C**) *Pf* NfnI structures show a different location of Fd at NfnI-L. (**B**) In the as-purified structure, Fd is docked between the helical bundle domain and the loop 371-391 in an "open" conformation. At this location, the side

chains of the residues 73-80 of the helical bundle domain of *Pf* NfnI are hydrogen bonded to the side chains of 8-13 and 88-97 of Fd (inset). (**C**) In the NADP(H) bound structure, Fd is docked to *Pf* NfnI at the location in which the side chains of the Fd residues 12-15 are hydrogen bonded to the side chains of the NfnI-L residues 43-46 (inset). Upon binding of NADP(H) to NfnI-L, the loop 371-391 is stabilized and the polar contacts between the side chains of *Pf* NfnI and Fd are disrupted.

Supplementary References

1 Wang, S., Huang, H., Moll, J. & Thauer, R. K. NADP+ reduction with reduced ferredoxin and NADP+ reduction with NADH are coupled via an electron-bifurcating enzyme complex in *Clostridium kluyveri*. *Journal of Bacteriology* **192**, 5115-5123 (2010).

2 Demmer, J. K. *et al.* Insights into Flavin-based Electron Bifurcation via the NADH-dependent Reduced Ferredoxin:NADP Oxidoreductase Structure. *Journal of Biological Chemistry* **290**, 21985-21995, doi:10.1074/jbc.M115.656520 (2015).

3 Mohsen, A. A., Rigby, S. E. J., Jensen, K. F., Munro, A. W. & Scrutton, N. S. Thermodynamic Basis of Electron Transfer in Dihydroorotate Dehydrogenase B from *Lactococcus lactis*: Analysis by Potentiometry, EPR Spectroscopy, and ENDOR Spectroscopy. *Biochemistry* **43**, 6498-6510 (2004).

4 Page, C. C., Moser, C. C., Chen, X. & Dutton, P. L. Natural engineering principles of electron tunnelling in biological oxidation-reduction. *Nature* **402**, 47-52 (1999).

5 Hagen, W. R. *et al.* Novel structure and redox chemistry of the prosthetic groups of the iron-sulfur flavoprotein sulfide dehydrogenase from *Pyrococcus furiosus*; evidence for a [2Fe-2S] cluster with Asp(Cys)3 ligands. *Journal of Biological Inorganic Chemistry* **5**, 527-534 (2000).

6 Conover, R. C. *et al.* Spectroscopic characterization of the novel iron-sulfur cluster in *Pyrococcus furiosus* ferredoxin. *Journal of Biological Chemistry* **265**, 8533-8541 (1990).

7 Ma, K. & Adams, M. W. Sulfide Dehydrogenase from the Hyperthermophilic Archaeon *Pyrococcus furiosus*: a New Multifuntional Enzyme Involved in the Reduction of Elemental Sulfur. *Journal of Bacteriology* **176**, 6509-6517 (1994).

8 Hagen, W. R. *Biomolecular EPR spectroscopy*. (CRC press, 2008).